THE JOURNAL OF PHYSICAL CHEMISTRY B

Article

pubs.acs.org/JPCB

Protein Conformation-Controlled Rebinding Barrier of NO and Its Binding Trajectories in Myoglobin and Hemoglobin at Room Temperature

Seongheun Kim and Manho Lim*

Department of Chemistry and Chemistry Institute for Functional Materials, Pusan National University, Busan 609-735, Korea

ABSTRACT: The effect of the solvent viscosity on the dynamics of NO rebinding to myoglobin (Mb) and hemoglobin (Hb) was examined by femtosecond (fs) time-resolved vibrational spectroscopy after photodeligation of NO from MbNO and HbNO in various viscous solutions at 283 K using a 580 nm excitation pulse. The rebinding kinetics of NO to both Mb and Hb were nonexponential, but their dependence on the solvent viscosity was different. The rate of NO rebinding to Mb increased with increasing solution viscosity, which was achieved by increasing the glycerol content in glycerol/water mixture. In contrast, the rate of NO rebinding to Hb was independent of the solution viscosity but faster than the fastest rate of NO rebinding observed in Mb. The dynamics of conformational relaxation of the protein after deligation were also measured by probing the evolution of the amide band. The effect of the solvent viscosity on the kinetics of conformational relaxation in both proteins was also quite different. The conformational relaxation of Mb became slower with increasing solution viscosity. On the other hand, the conformational relaxation of Hb was independent of the solution viscosity but slower than the slowest kinetics of Mb. The inverse correlation in the kinetics of conformational relaxation and NO rebinding suggests that the barrier of NO rebinding increases as the conformation of the protein relaxes toward the deligated structure after NO dissociation. The rebinding kinetics of NO to both proteins was well described by a kinetic model incorporating a time-dependent barrier for rebinding and exponential translocations between three states for dissociated NO.

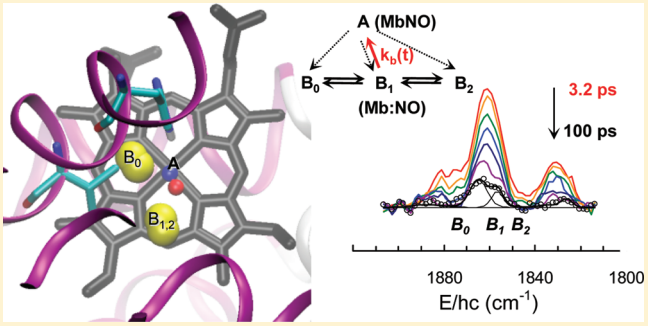

I. INTRODUCTION

The binding of small diatomic ligands, such as O_2, CO, and NO, with the heme prosthetic group in myoglobin (Mb) and hemoglobin (Hb) has been used as a model system to examine how the protein function is related to its structure and dynamics.[1−9] Studies of geminate rebinding (GR) of a dissociated ligand after photolysis of ligand-bound heme proteins showed that the GR is coupled strongly to the protein motions and can probe how the protein motions control ligand binding.[5,10−14]

For MbCO under physiological conditions, the GR yield is too low (~4% in room temperature aqueous solution),[3] and the rebinding dynamics of dissociated CO is dominated by bimolecular kinetics after release into solution.[3] Therefore, MbCO under physiological conditions is more useful for examining the conformational relaxation of heme proteins after deligation. In contrast, the GR of NO to Mb in room temperature solution is almost complete on a picosecond (ps) time scale. Accordingly, NO rebinding has been used to examine the nature of the underlying protein dynamics related to ligand binding.[6,11−18]

The GR of NO to Mb is strongly nonexponential, even in room temperature aqueous solution, and many explanations for the nonexponential kinetics have been proposed.[11−15,19] Rebinding is nonexponential when there is a distribution of rebinding barriers due to protein conformational substates that equilibrate more slowly than rebinding[1,5,20−22] or a time-dependent barrier resulting from protein relaxation on a similar time scale to that of rebinding.[11,13,14,22−28] A structure specific probe like vibrational spectroscopy is advantageous for delineating a possible mechanism between various proposed explanations.[12−14] Recently, we showed that the two conformational substates of MbNO in D_2O have the same GR kinetics by measuring the recovery kinetics of bound NO after photolysis using fs vibrational spectroscopy.[13] This suggests that the nonexponential GR of NO to Mb in an aqueous solution at room temperature arises not from the static inhomogeneity of MbNO but from conformational relaxation and/or multiple sites for the dissociated NO. More recently, by directly probing the photodeligated NO from MbNO by fs IR spectroscopy, we observed three states for the deligated NO within Mb and determined their time-dependent behaviors. By analyzing this state-specific kinetics and recovery dynamics of bound NO, we proposed that the nonexponential GR kinetics of NO arises from the growing barrier for rebinding due to the

Received: January 6, 2012
Revised: March 17, 2012
Published: April 30, 2012

dx.doi.org/10.1021/jp300176q | *J. Phys. Chem. B* 2012, 116, 5819−5830

conformational relaxation of Mb as well as the translocations of NO between the three states.[14]

The temperature-dependent and viscosity-dependent kinetics of NO rebinding were examined to determine the effect of the protein motion on ligand binding in detail.[12,28] Shreve et al. reported that the GR of NO to Mb at room temperature became faster with increasing glycerol content in the solvent.[12] The viscosity-dependent kinetics was analyzed to have two dominant rate processes. The faster rate contributes more with a negligible change in rate, but the slower rate increases with a diminishing contribution as the solvent viscosity is increased. The viscosity-dependent kinetics was attributed to two distinct states of photodissociated NO (denoted as B_1 and B_2 analogous to photodissociated CO).[12,29] The observed kinetics was suggested to follow a parallel model, where the rebinding rate of B_1 is independent of the solution viscosity and the rate of B_2 increases with the solution viscosity.[12] Recently, Champion and co-workers performed careful temperature-dependent studies of NO rebinding to heme, Mb, and Mb mutants using fs electronic spectroscopy and suggested a harpoon mechanism for NO binding to heme where the proximal barrier, which is dominated by the heme Fe out-of-plane conformation, makes a negligible contribution to NO rebinding.[28] They suggested that the standard three-state serial kinetic model with a modified initial condition can explain the observed temperature-dependent behavior in NO rebinding.[28] They concluded that in the two kinetic phases observed in Mb the temperature-independent faster rate results from the rebinding of NO from the primary docking site (denoted as B), and the temperature-dependent slower one represents the motion of NO from a more distant site like the Xe4 pocket[30] to the B site. The fast rebinding in a ps time scale was attributed to the reactant-like transition state for NO binding,[31] in which the NO molecule binds to the heme Fe in out-of-plane position without waiting for Fe motion into the heme plane by thermal fluctuations.[28] Although the suggested model was consistent with the observed recovery kinetics of the population of MbNO, to be self-consistent, it needs to satisfy the kinetic behavior of the dissociated NO in the various states observed in fs vibrational spectroscopy.[28] The above-mentioned kinetic models have not been tested rigorously with the kinetics of the dissociated NO.

According to time-resolved near IR absorption spectroscopy, the spectral shift of band III, representing the out-of-plane Fe motion at room temperature, evolves over a wide time scale and is retarded in a viscous glycerol/water mixture. This suggests that protein relaxation is slowed by the addition of glycerol to the solvent.[32] The conformational relaxation of Mb in D_2O at room temperature was also monitored by the time-dependent change in the protein amide bands after the photodeligation of MbCO.[33−35] Transient spectra in the amide region of Mb in D_2O evolve with a time constant of 6−12 ps, suggesting that the final deligated conformation is substantially formed on a ps time scale. In the transient kinetics traces of Mb, the main change in the amide band I decays with almost the same time constant (8−9 ps) as that in amide band II.[35] The solvent viscosity can retard the ps conformational relaxation probed in the amide band. However, no systematic study has been carried out on the dynamics of the amide band in Mb after photodeligation at room temperature as a function of the solvent viscosity. Time-resolved vibrational spectroscopy can measure simultaneously the evolution of the amide band and the GR dynamics of NO. It also shows site-specific kinetics,[12] which can be used to envision the pathway of dissociated NO.[14]

The global tertiary structure of the subunit in the tetrameric Hb, which consists of two α chains and two β chains, is similar to that of Mb.[36,37] Therefore, a comparative study of Mb and Hb can reveal the effect of the quaternary structure on ligand binding and conformational relaxation. Although the GR of NO to Hb has been reported, the viscosity-dependent GR dynamics of NO to Hb have not been measured. The viscosity-dependent evolution of the amide band and GR kinetics of NO in Hb can unveil the conformational relaxation of Hb on a ps time scale as well as how the NO rebinding is affected by the ps conformational relaxation of Hb, which may be affected by the quaternary structure.

Here, the GR dynamics of NO to Mb and Hb in a range of viscous solutions and their conformational relaxation were measured simultaneously as a function of the solvent viscosity. An inverse correlation was found in the kinetics of the NO GR and conformational relaxation. The viscosity-dependent GR kinetics of NO to Mb and Hb were well described by a kinetic model incorporating a time-dependent rebinding barrier and exponential translocations of the dissociated NO between the three states.

II. MATERIALS AND METHODS

The fs time-resolved mid-IR spectrometer used in this study is described in detail elsewhere.[13] Briefly, two identical home-built optical parametric amplifiers (OPA), which were pumped by an amplified pulse from a commercial Ti:sapphire oscillator/amplifier system at a 1 kHz repetition rate, were used to generate a visible pump pulse[38] and a tunable mid-IR probe pulse.[39,40] The optically delayed visible pump pulse, which was set to 580 nm with a 3 μJ energy, photoexcited the sample, and the probe pulse measured the transient mid-IR absorbance of the sample. The transmitted broadband probe pulse was detected using a 64-element N_2(l)-cooled HgCdTe array detector mounted on a 320 mm monochromator with a 150 lines/mm grating, showing a spectral resolution of ca. 1.1 or 1.4 cm^{-1}/pixel at 1600 or 1800 cm^{-1}, respectively. The transient spectra spanning 110 cm^{-1} are a superposition of two 64-point spectra that overlap by a few elements. The monochromator was calibrated against a water vapor signal in the spectral region examined. To obtain the isotropic spectrum, the polarization of the pump pulse was set to the magic angle (54.7) relative to the probe pulse. The pump-induced change in the absorbance of the sample, ΔA, was determined by chopping the pump pulse at half the repetition frequency of the laser and calculating the difference between the pumped and unpumped absorbance. Chopping the excitation light pulse afforded greater immunity to a long-term instrumental drift. The excellent short-term stability of the IR light source (<0.5% rms) made it possible to routinely obtain $<1 \times 10^{-4}$ rms in absorbance units after 0.5 s of signal averaging without single shot referencing with an independent detector. The pump spot was made larger than the probe spot to ensure spatially uniform photoexcitation across the spatial dimensions of the probe pulse.[41] A moderate pump energy with an enlarged photolysis beam size also minimized the spatial thermal effects in the sample. The time resolution achieved in this study, which was determined by the transient absorption of a Si wafer, was <180 fs full width at half-maximum.

A 6−10 mM MbNO sample was prepared by dissolving lyophilized skeletal horse Mb (Sigma) in deoxygenated D_2O

dx.doi.org/10.1021/jp300176q | J. Phys. Chem. B 2012, 116, 5819−5830

(Merck, 99.9% D), 48 wt % glycerol/D_2O (G/W), 64 wt % G/W, and 73 wt % G/W solutions buffered with 0.2 M potassium phosphate (pD 7.4), reducing with a 2-fold excess of freshly prepared $Na_2S_2O_4$ (Aldrich), and adding an equivalent quantity of a 0.1 M degassed $NaNO_2$ (Aldrich) solution in the presence of an equimolar quantity of 0.1 M $Na_2S_2O_4$.[42] Various 2−2.5 mM HbNO (8−10 mM in heme) viscous solutions were prepared using the same method employed to prepare MbNO using lyophilized human Hb (Sigma). Samples with $Na^{15}NO_2$ were also prepared to assist in the vibrational band assignment. All sample preparations were carried out in an ice bath to minimize thermal denaturation. Light scattering sources such as dust particles and denatured protein aggregates were removed by filtering the MbNO and HbNO samples through a 0.45 and 5 μm membrane filter, respectively. After filtration, the sample was loaded in a gastight 6 μm path length rotating or 100 μm path length flowing sample cell with two 2 mm thick CaF_2 windows. The rotating sample cell tends to have higher noise due to inhomogeneous scattering from the cell window, and the flowing cell requires a path length >50 μm to flow a concentrated protein sample. The flowing cell was used to collect the spectra of the deligated NO. The rotating cell was used for the spectra of bound NO to minimize the strong background absorption arising from the amide I band and water near the absorption for bound NO. During data collection, the sample cell was rotated or flowed fast enough to ensure a fresh volume of the sample to be photoexcited by subsequent laser pulses. Throughout the experiments, the integrity and concentration of the sample were checked routinely by UV−vis and FT-IR spectroscopy. A D_2O solvent was used to avoid the strong IR absorption of H_2O in the spectral region of interest. The sample cell temperature was kept at 283 ± 1 K using a circulating bath connected to an aluminum sample-cell housing block.

III. RESULTS

Figure 1 shows representative time-resolved vibrational spectra of photodeligated MbNO and HbNO in D_2O and 73 wt % G/W solutions at 283 K. Since this study focused on the population changes in the deligated protein after photolysis, which occurs in later than a few ps, the data at pump−probe delay times ≥0.3 ps were used in data analysis to avoid the contributions from the truncated free induction decay of the vibrational band of the bound NO and from the coherent signals occurring when the pump−probe pulses are overlapped.[43,44] The negative-going features (bleach), resulting from the loss of bound NO (denoted as A state), appear to be faster than the time resolution of the instrument, confirming the ultrafast photodeligation of NO from the heme proteins.[6] Care was taken to extract the time evolution of the bleach free from the signals from the thermal and conformational changes in the protein because the probed spectral region overlapped with the amide I and II bands, which are sensitive to temperature and protein conformation.[13,33−35,45,46] The vibrational band of the bound NO was assigned using isotope-labeled $Mb^{15}NO$ and $Hb^{15}NO$.[13] The NO band was described well by the sum of two Gaussians. The featureless background as well as the amide bands was modeled using a quadratic polynomial plus a few Gaussians and subtracted from the spectra for clarity.[13] The position of the NO band in MbNO and HbNO was shifted slightly to a higher frequency with increasing glycerol content in the solvent, but its spectral width was preserved. The negligible change in the spectral characteristics suggests that the viscous solvent has an insignificant effect on the surrounding structures of the distal pocket interacting with the bound NO. The magnitude of the bleach is proportional to the population of deligated protein, and its decay arises from NO rebinding to the deligated protein. Since bimolecular rebinding proceeds on a ms time scale,[3] the observed decay on the ps time scale can be attributed solely to the GR. The magnitude of the bleach in Mb decreases while maintaining its shape. The magnitudes of the two Gaussian components for the NO band in Mb decayed at the same rate, suggesting that the two conformational substates of MbNO represented by two Gaussian bands have the same rebinding rate. A small band at 1584 cm^{-1} was added when fitting the spectra of MbNO in D_2O.[13] This band has ∼3% of the magnitude of the main band and decays at the same rate as the main band. Nevertheless, this was ignored hereafter because it becomes even smaller in viscous solvents. Two Gaussian components in Hb, each component with a 50 ± 2% contribution, decayed slightly differently: one component in blue side decayed faster than the other in red. Each component possibly corresponds to the α or β subunit of Hb. Detailed analysis of HbNO will be published elsewhere.[47]

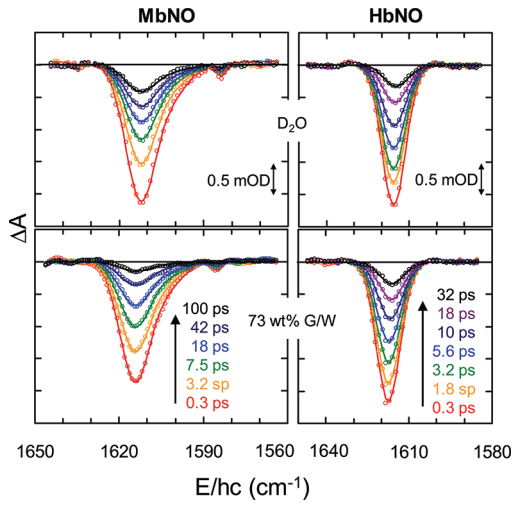

Figure 1. Representative time-resolved vibrational spectra of photolyzed MbNO (left panels) and HbNO (right panels) in D_2O (top panels) and 73 wt % G/W solutions (bottom panels) at 283 K. The data (○) was modeled (solid line) using the sum of two Gaussians. The unit in the *y*-axis is the difference in optical density (OD; 1 mOD = 10^{-3} OD) between the photolyzed and unphotolyzed samples. The pump−probe delays are 0.3−100 ps in MbNO and 0.3−32 ps in HbNO and are color-coded in each protein. For clarity, a quadratic polynomial and a few Gaussians modeling signals due to thermal and conformational relaxation were subtracted from the measured spectra (see text). For Mb in D_2O, a small Gaussian was also included to fit the small shoulder at 1584 cm^{-1}.

As reported before,[13] the NO band in MbNO in D_2O consists of two overlapping vibrational bands: a major band at 1611 cm^{-1} and a shoulder band at 1598 cm^{-1}. It is well compared with vibrational band at cryogenic temperature measured by Nienhaus et al.,[48] which is located at 1614 and 1607 cm^{-1}. The band at 1614 and 1607 cm^{-1} was assigned to the NO band in A_1 and A_3 conformation of MbNO, respectively.[48] In A_1 and A_3 conformation, the imidazole side chain of His-64 is neutral and resides in the distal pocket. The His-64 imidazole in A_3 conformation is located more deeply in the heme pocket than that in A_1 conformation, resulting in a

dx.doi.org/10.1021/jp300176q | J. Phys. Chem. B 2012, 116, 5819−5830

stronger interaction between the His-64 side chain and the ligand.[48] The vibrational band at cryogenic temperature is narrower and less separated than that at 283 K. However, since two vibrational bands at 283 K are similar to those found at cryogenic temperature, the same assignment was made for two bands at 283 K: 1611 cm^{-1} band to A_1 conformation and 1598 cm^{-1} band to A_3.

The kinetics of the GR of NO to Mb and Hb in a range of viscous solvents was obtained by global fitting of each complete set of 20 bleach spectra for a given sample using a global Marquart–Levenberg nonlinear least-squares algorithm[49] and is shown in Figure 2. Although the center wavenumbers, line

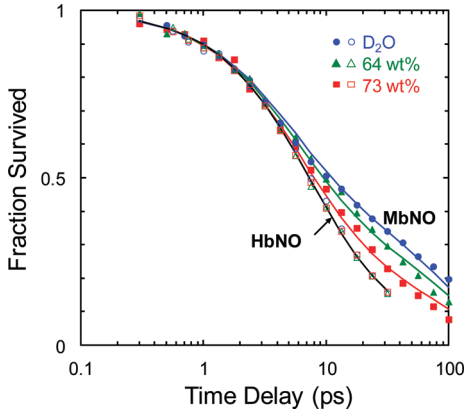

Figure 2. Kinetics of geminate rebinding of NO after photodeligation of MbNO (filled symbols) and HbNO (open symbols) in various solutions at 283 K. The data were shown for D_2O (blue circles), 64 wt % G/W (green triangles), and 73 wt % G/W solutions (red squares). The solid lines are the fits to a function describing the kinetic model incorporating a time-dependent rebinding barrier with exponential translocations between the three B states (see text). The fitted parameters are summarized in Table 2.

widths, and relative amplitude of the two Gaussians for the NO band were optimized globally, the magnitude of the band was optimized at each delay time to determine the population change in the deligated protein. The global fitting of the complete set of bleach spectra warrants more accurate spectral parameters, facilitating the reliable recovery of the population change of the deligated protein. As shown in Figure 2, the rate of NO rebinding to Mb increased with increasing solvent viscosity. In contrast, NO rebinding to Hb was independent of the solvent viscosity and was faster than that to Mb in the 73 wt % G/W solution, which was the fastest NO rebinding in Mb measured in this study. The gradual increase in the NO rebinding rate to Mb with increasing glycerol content in the solvent is consistent with previous reports using transient electronic absorption measurements.[12] The kinetics of NO rebinding cannot be described by a single exponential and requires a nonexponential function.

Figure 3A shows the time-resolved vibrational spectra of photodetached NO from MbNO in a 48 wt % G/W mixture at 283 K. A featureless background, arising from a solvent absorption change due to thermal relaxation of the photo-excited protein, was modeled with a quadratic polynomial and subtracted for clarity. The spectral characteristics of the NO bands were very similar to those observed in MbNO in D_2O. Therefore, the transient spectra were analyzed in the same way as in MbNO in D_2O: three evolving bands (denoted B_0, B_1, and B_2) plus their red-shifted replicas for vibrationally excited NO

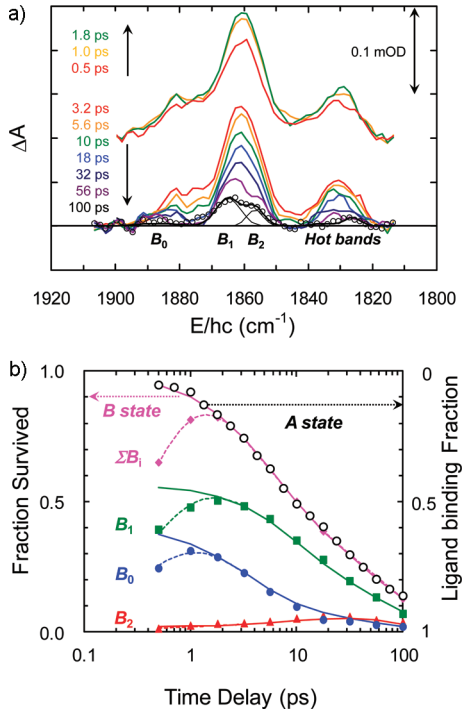

Figure 3. (a) Time-resolved vibrational spectra of the stretching mode of NO after the photolysis of MbNO in 48 wt % G/W mixture. Data from 0.5 to 1.8 ps were offset to avoid overlap. For clarity, the featureless background signals due to thermal relaxation of solvent have been subtracted from the measured spectra. The spectrum at 100 ps was decomposed into three Gaussians labeled B_0, B_1, and B_2 plus a red-shifted replica of these Gaussians (○, data; —, fit). The red-shifted replicas were assigned to hot bands of B_0, B_1, and B_2 bands. (b) Time dependence of the integrated absorbance of the B state (filled symbols) and A state (open circles) of MbNO in 48 wt % G/W solution. This is well described by the kinetics scheme incorporating a time-dependent rebinding barrier from B_1 and exponential translocations between the three B states (see text). The dotted and solid lines represent the fit with an initial increase and the population of the corresponding B states, respectively. The integrated absorbance of the B state is sum of the ground state absorbance and the excited state absorbance for the corresponding state (see text).

(v = 1).[14] As suggested,[50] the three bands arise from different positions and/or orientation of the NO within the heme pocket in a given conformational substate of the protein. The vibrationally excited NO (v = 1) contributes to the integrated absorbances for transitions from both the first excited state (A_e) and the ground state (A_g). Within harmonic oscillator approximation, the integrated absorbances are related to the populations of the first excited state (n_e) and the ground state (n_g) by $A_e = 2\varepsilon n_e$ and $A_g = \varepsilon(n_g - n_e)$, where ε is the integrated absorption cross section for the ground state transition,[14] resulting in $(n_g + n_e) = (A_e + A_g)/\varepsilon$. Therefore, the population of a certain state is related to the sum of absorbances of the fundamental and hot bands for the given state. Using a reactive molecular dynamics simulation on NO rebinding to Mb, Karplus and co-workers showed that the NO rebinding to Mb is independent of NO vibrational energy.[25] Here, we assumed that the vibrationally excited NO has the same rebinding kinetics as the ground state NO. Thus, the hot band contribution was merely added to the integrated area of the corresponding B state.[14,47] When the kinetics of hot bands were fitted, the recovered population of vibrationally excited NO and

dx.doi.org/10.1021/jp300176q | J. Phys. Chem. B 2012, 116, 5819–5830

vibrational relaxation time was 17 ± 3% and 210 ± 50 ps, respectively, which is the same as those in D_2O. The kinetics of the integrated area for the three B states shown in Figure 3B is similar to that found in MbNO in D_2O, except for the faster decay in a 48 wt % G/W solution. Similar to an analysis of the dissociated NO from MbNO in D_2O,[14] various kinetics schemes were used to describe the kinetic behavior of the B states. A kinetics scheme containing a time-dependent rebinding from B_1 and exponential translocations between three B states (see Figure 4) was found to be most consistent with the data. As reported previously,[14] the time-dependent rebinding was modeled by introducing a time-dependent barrier $E(t)$ into the Arrhenius equation, $k(t) = A \exp[-E(t)/RT]$, with $E(t) = (E_0 - E_{eq}) \exp(-k_{bar}t) + E_{eq}$.[11] Here, A, R, T, and k_{bar} represent the Arrhenius prefactor, gas constant, absolute temperature, and rate constant for the growth of the barrier height from its initial height, E_0, to its equilibrium value E_{eq}, respectively. When fitted, the translocations between B_0 and B_2 were negligible and were ignored in the final fitting. Interestingly, the fitted rate constants for the translocations between the three B states in a 48 wt % G/W solution were indistinguishable from those in D_2O, and only time-dependent rebinding is faster in the viscous solution. Therefore, in the final fitting, the kinetic behavior of the three B states under the constraint of recovering the A-state kinetics for both samples in D_2O and 48 wt % G/W solutions were fitted globally. In the global fitting, the kinetics for both samples were fitted to a kinetics scheme simultaneously while all the rate parameters in the kinetics scheme except for the rate constant for the growth of the rebinding barrier were kept common. As shown in Figure 3B, the kinetics scheme with global fitting well describes the time dependence of the A state and three B states for MbNO in a 48 wt % G/W solution, simultaneously. The fitted parameters shown in Figure 4 were virtually identical to those obtained from the fitting data of D_2O alone. The recovered parameters for the time-dependent barrier were $A = (2.1 \pm 0.2) \times 10^{11}$ s^{-1} and $E_{eq} = 1.5 \pm 0.1$ kcal/mol for both solvents. While fitting the data, we found that the rebinding kinetics alone cannot determine both heights for the varying barrier, E_0 and E_{eq}, uniquely. In principle, there is no barrier initially, i.e., $E_0 = 0$ kcal/mol. A previous experiment on the rebinding of NO to Mb reported that $E_0 = 0.027$ kcal/mol.[11] Either value resulted in almost the same values for the remaining rate parameters. Here, for the sake of the simplicity, we used the literature value, $E_0 = 0.027$ kcal/mol. The fitted k_{bar} was $(14 \pm 1$ ps$)^{-1}$ in D_2O and $(17 \pm 1$ ps$)^{-1}$ in the 48 wt % G/W mixture. The initial partitioning of photodetached NO was fitted to 42 ± 4% in B_0, 56 ± 7% in B_1, and 2 ± 1% in B_2, which is also identical to those recovered in the data of D_2O alone. The fitted initial rise time of the integrated B-state absorbance, 0.6 ± 0.2 ps, is also the same as that in the D_2O data. This was attributed to a rearrangement of the protein after deligation.[14,51]

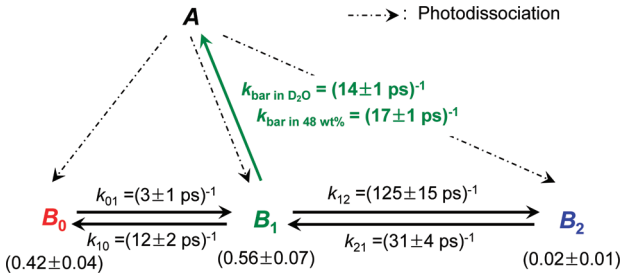

Figure 4. Kinetics scheme used to fit the kinetics of the B states and A state and their best-fit parameters for MbNO in D_2O and 48% G/W solutions. The dot-dashed arrows represent the pathways of the photodetached NO from MbNO, black solid arrows represent translocations between the B states, and the green solid arrow represents geminate rebinding. The k_{ij} represents the rate constant for the translocation from the B_i to B_j states. The translocations between B_0 and B_2 were negligible and were ignored. The rate constant for the growth of the rebinding barrier (k_{bar}) is given in the rebinding from B_1 to A. The parameters for the time-dependent barrier were $A = 2.1 \times 10^{11}$ s^{-1}, $E_0 = 0.027$ kcal/mol, and $E_{eq} = 1.5$ kcal/mol for both solvents. The values shown in the parentheses is the nascent partitioning of the photodeligated NO. The quoted uncertainties reflect the estimated experimental error.

The rebinding kinetics of NO to the heme proteins measured by probing the recovery of the bound NO population (A state) was described using several nonexponential functions, such as a biexponential function, a stretched exponential function, and a function with a time-dependent rebinding rate incorporating a time-dependent barrier arising from protein relaxation on the same time scale as the rebinding process.[6,11−14,16,17,24,52,53] These nonexponential functions fit the rebinding kinetic quite well. Table 1 lists the recovered parameters from these fits for comparison with values reported in the literature. On the other hand, to fully describe the dynamics of GR for the dissociated NO, the translocations among the B states should be considered. This is because the dissociated NO is distributed into three states and interconverts in these states on the same time scale of the GR. As shown above, the transition rates between the three B states are virtually independent of the solvent viscosity and only the rate for the barrier growth changes. This is consistent with a previous report showing that the transition rates between the two B states of MbCO and

Table 1. Fitted Parameters for Geminate Rebinding of NO to Mb and Hb at 283 K

		biexponential[a]			stretched exponential[b]			time-dependent barrier[c]			
sample	solvent	a_1	τ_1 (ps)	τ_2 (ps)	a_2	τ_3 (ps)	β	A (ps^{-1})	E_0[d] (kcal/mol)	E_{eq} (kcal/mol)	$1/k_{bar,b}$ (ps)
	D_2O	0.53	4.8	109	0.8	12	0.70				15
MbNO	64 wt % glycerol	0.50	5.0	66	0.87	14	0.72	0.13	0.027	1.5	19
	73 wt % glycerol	0.55	5.3	52	0.93	14	0.73				25
HbNO	all solvents	0.54	5.6	29	0.87	9	0.92	0.14	0.000 67	1.6	44

[a]The biexponential function, $a_1 \exp(-t/\tau_1) + (1 - a_1) \exp(-t/\tau_2)$. [b]The stretched exponential function, $a_2 \exp(-(t/\tau_3)^{\beta}) + (1 - a_2)$. [c]The time-dependent barrier, the barrier decay rate $k(t) = A \exp(-E(t)/RT)$, with $E(t) = (E_0 - E_{eq}) \exp(-k_{bar,b}t) + E_{eq}$, where $k_{bar,b}$ is the rate constant for the growth of the barrier from its initial height E_0 to its equilibrium value, E_{eq}, when the recovery of the bleach is fitted without considering kinetics of the individual B states. The recovered $k_{bar,b}$ is slightly smaller than the k_{bar}, the recovered parameter while considering the kinetics of individual B state (shown in Table 2). A is an Arrhenius prefactor. [d]E_0 is from ref 11.

dx.doi.org/10.1021/jp300176q | J. Phys. Chem. B 2012, 116, 5819−5830

HbCO was almost independent of the solvent viscosity.[54] We also measured the time-resolved vibrational spectra of photodissociated NO from HbNO in D_2O. Three B states for dissociated NO were identified, and the GR of NO to Hb was also well described by the kinetics scheme incorporating the time-dependent rebinding from B_1 and time-independent transitions between the three B states,[14] the same kinetics scheme used to describe the GR of NO to Mb.[47] Here, the same kinetics scheme (shown in Figure 4) was employed to fit the A-state kinetics of MbNO and HbNO in various viscous solutions. Since the transition rates between the B states of Mb and Hb are almost independent of the solvent viscosity,[54] rebinding kinetics of a given protein in various solutions was globally fitted by adjusting the parameters for time-dependent barrier while the rate constants of the translocations between the three B states of NO in the G/W solutions were set to be the same as those of the corresponding protein in D_2O.[14,47] For a given protein, parameters for the rebinding barrier were fitted globally except k_{bar}. Table 2 lists the recovered parameters including k_{bar} in various solvents. As shown in Figure 2, the fit

Table 2. Fitted Parameters for the Growth of the Rebinding Barrier from B_1 State in the Kinetics Model Incorporating a Time-Dependent Rebinding from B_1 and Exponential Translocations between Three B States[a]

sample	solvent	time-dependent barrier from B_1 state			
		A (ps^{-1})	E_0[b] (kcal/mol)	E_{eq} (kcal/mol)	$1/k_{bar}$ (ps)
	D_2O				14 ± 1
MbNO	64 wt % glycerol	0.21 ± 0.02	0.027	1.5 ± 0.1	17 ± 1
	73 wt % glycerol				23 ± 2
HbNO	all solvents	0.18 ± 0.02	0.000 67	1.6 ± 0.1	39 ± 3

[a]Kinetics of A state for a given protein in various viscous solutions was simultaneously optimized in the fitting. [b]E_0 is from ref 11.

reproduces the kinetics of GR of NO to both proteins in various solutions quite well. The k_{bar} in Mb increases gradually from $(14 \pm 1\ ps)^{-1}$ to $(23 \pm 2\ ps)^{-1}$ with increasing solvent viscosity. In contrast, the k_{bar} in Hb is independent of the solvent viscosity and was fitted to $(39 \pm 3\ ps)^{-1}$, which is much slower than that in Mb.

As mentioned above, the amide bands are sensitive to the conformational change in the protein after deligation and were used to probe the dynamics of conformational relaxation of photodeligated heme proteins.[33−35] They overlapped with the vibrational band of NO in MbNO and HbNO as well as the broad solvent band that is sensitive to the solvent temperature. The kinetics of the amide band in MbNO and HbNO can be probed by carefully selecting an amide band that is minimally contaminated by any contribution from the NO vibrational band or thermal evolution of the solvent band. Since the solvent band is broad, the thermal evolution of the solvent band is observed as a featureless background. The NO vibrational band was identified by comparing the spectra of the ^{15}NO-bound protein with that of the ^{14}NO-bound protein. Figure 5 shows the transient vibrational spectra of isotope labeled (^{14}NO or ^{15}NO) MbNO and HbNO after photodeligation of the corresponding proteins in D_2O at a pump−probe delay of 1 ps.

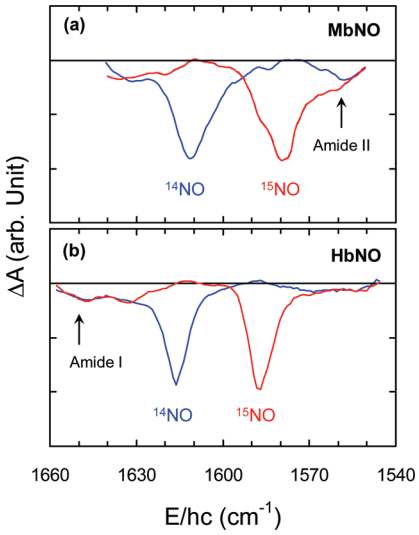

Figure 5. Time-resolved vibrational spectra of photodeligated (a) MbNO and (b) HbNO in D_2O probed at the pump−probe delay of 1 ps. The blue and red solid lines represent the spectra of the ^{14}NO and ^{15}NO bound proteins, respectively. The arrows point to spectral features of Mb and Hb that were used to probe the conformational changes in the protein after photodeligation.

A distinct feature in amide band can be characterized readily without any contribution from the featureless background signal due to thermal evolution of the solvent band. An appropriate feature in amide band of each protein that was well separated from the NO vibrational band and minimally affected by the featureless background signal from thermal relaxation was chosen because the main features in the amide I and II bands of Mb have similar decay kinetics.[35] For MbNO, the feature at 1558 cm^{-1} in amide II band showed a distinct band that was well separated from the NO band. On the other hand, for HbNO, the feature at 1650 cm^{-1} in amide I band showed a well-separated distinct band that can be characterized clearly. These bands, likely resulting from changes in amide band due to evolving conformation of the protein, were used to monitor the kinetics of conformational relaxation of the corresponding protein after deligation. Figure 6 shows the decay kinetics of the distinct features in the amide bands of MbNO and HbNO after the photodeligation of NO in various solvents. The decay kinetics was well described by an exponential function. The decay rate of the feature in the amide band in Mb decreased with increasing solvent viscosity and is described well by a single-exponential decay function with a lifetime of 5.4, 6.7, and 10 ps for MbNO in D_2O, 64 wt % G/W, and 73 wt % G/W solutions, respectively. In contrast, the decay of the feature in the amide band of Hb was independent of the solvent viscosity and is described well by an exponential function with a lifetime of 15 ps. Clearly, the ps conformational relaxation in Mb after the photodeligation of NO was retarded by the viscous solvent, whereas that in Hb was relatively unaffected by the solvent viscosity on the ps time scale. The deligated heme proteins undergo conformational relaxation over wide range of time scales ranging from femtoseconds to many seconds.[19,55,56] Although the conformational relaxation in Hb at the early time was negligibly affected by the solvent viscosity, it could be influenced by the solvent viscosity on a longer time scale.

dx.doi.org/10.1021/jp300176q | J. Phys. Chem. B 2012, 116, 5819−5830

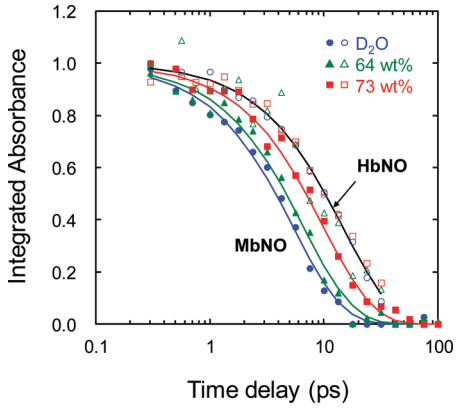

Figure 6. Time-resolved IR absorption kinetic traces of MbNO (filled symbols) in the amide II region at 1558 cm^{-1} and HbNO (open symbols) in the amide I region at 1650 cm^{-1} after photolysis of the corresponding proteins in D_2O (blue circles), 64 wt % G/W (green triangles), and 73 wt % G/W (red squares) solutions. The symbols correspond to the experimental data, and the solid lines represent the fits to the data with single-exponential functions.

IV. DISCUSSION

Viscosity Dependence. In MbNO, the NO rebinding rate increased with increasing solvent viscosity and the conformational relaxation rate decreased. In HbNO, both NO rebinding and conformational relaxation were independent of the solvent viscosity. The rate of NO rebinding to Hb was faster than the fastest rate of rebinding to Mb, and the conformational relaxation of Hb was slower than the slowest relaxation in Mb. Clearly, there is an inverse correlation in the kinetics between NO rebinding and conformational relaxation, suggesting that conformational relaxation retards NO rebinding. The rebinding barrier was suggested to grow with conformational relaxation because the protein undergoes conformational relaxation toward the deligated structure immediately after photodeligation, and rebinding requires reversal of the relaxed structure toward the ligated form.[11] The observed inverse correlation is consistent with the notion that the rebinding barrier increases with conformational relaxation.

Upon the deligation of a diatomic ligand from a heme protein, the protein conformation relaxes toward the structure for the deligated protein. A conformational change includes a rearrangement of the residues surrounding the distal pocket as well as the out-of-plane motion of the Fe in heme. Although the initial out-of-plane Fe motion occurs within 1 ps, the time scale for the latter stage of Fe motion ranges from the ps to ms scale due to the strong coupling between the primary Fe motion to the overall tertiary conformation.[32,57,58] For a monomeric polypeptide, Mb, its overall tertiary motion can be affected strongly by the solvent viscosity. The slower conformational relaxation of Mb in viscous solvents on the ps time scale clearly demonstrates the strong coupling between the ps conformational change in Mb and the motion of the solvent.[32] In Hb, tertiary relaxation is accompanied by the allosteric R → T transition. Tertiary motion of Hb was found to be influenced by its quaternary structure[59] and conformational relaxation of Hb occurring before 1 μs is purely tertiary.[60] The slower ps conformational relaxation in Hb suggests that the ps conformational motion of Hb might be coupled to the quaternary motion. The time scale for quaternary motion is much slower than that for tertiary motion because quaternary motion involves systematic motion of the tertiary units, such as the allosteric R → T transition. The viscosity-independent kinetics of the NO rebinding and the ps conformational relaxation of Hb suggests that most of the NO rebinds faster than the conformational relaxation that increases the NO rebinding barrier significantly. Hence, NO rebinding is faster in Hb. The conformation of Hb is likely to be reversed toward the ligated structure without undergoing any significant conformational relaxation toward a deligated structure that increases the NO rebinding barrier. Quaternary contact in Hb is likely to be responsible for the negligible coupling between the solvent viscosity and dynamics of NO rebinding to Hb, occurring in <50 ps.

Kinetic Model for NO Rebinding. The kinetics for the recovery of the A state, which represents the population of the NO-ligated protein, after photodeligation can be described readily using a range of nonexponential functions. Some of these are listed in Table 1 along with their fitted parameters. For example, the biexponential fit for the GR of NO to Mb revealed a fast rate constant of $(5.0 \pm 0.3\ ps)^{-1}$, which was almost independent of the solvent viscosity and a slow rate constant increasing from $(110\ ps)^{-1}$ to $(52\ ps)^{-1}$ with increasing solvent viscosity. This is consistent with the kinetics obtained by probing the recovery of the ground electronic state of MbNO.[11] The GR of NO to Hb showed a fast rate constant of $(5.6\ ps)^{-1}$, which was similar to that in Mb, as well as a slow rate constant of $(29\ ps)^{-1}$, which was even faster than the corresponding slowest rate observed in Mb. The GR kinetics could also be described by the time-dependent barrier for rebinding.[11] In the time-dependent barrier model, the rate constant for growth of the rebinding barrier of NO to Mb decreased from $(15\ ps)^{-1}$ to $(25\ ps)^{-1}$ with increasing solvent viscosity. Although the rate was slightly slower than that obtained by including the translocations between the three B states (shown in Table 2), the trend was consistent with the notion that the rebinding barrier increased as the protein conformation toward the deligated form and the conformational relaxation is retarded by the viscous solvent. The rate constant for the growth of the NO rebinding barrier to Hb, independent of viscosity, was $(44\ ps)^{-1}$, which was even smaller than the smallest rate constant in Mb. This suggests that the ps conformational relaxation is retarded more by the quaternary structure of Hb than the viscous solvent. Clearly, the recovery kinetics of the A state alone cannot differentiate various nonexponential kinetic models.

Femtosecond vibrational spectroscopy revealed the deligated NO to be distributed between the three states with each state having its own kinetics. A successful kinetic model for NO rebinding should be able to describe the time-dependent behaviors of these three states because they can translocate between and rebind from the three states. As mentioned, when various kinetics schemes were tried to describe the kinetic behavior of the dissociated NO, the kinetics scheme with the time-dependent rebinding from B_1 and time-independent translocations between the three states was most consistent with the kinetic behavior of the deligated NO. On the basis of the temperature-dependent studies of NO recombination to Mb and Mb mutants using ultrafast visible pump−probe spectroscopy, Champion and co-workers observed fast and slow NO rebinding processes above 200 K and described the A-state kinetics of MbNO and its mutants by proposing a kinetics model with temperature-independent rebinding from the B state that exhibits temperature-dependent translocation with a X state.[28] The B and X state was assigned to the NO trapped in

dx.doi.org/10.1021/jp300176q | J. Phys. Chem. B 2012, 116, 5819−5830

the distal heme pocket and in or near the Xe4 site, respectively. They concluded that this three-state (A, B, and X) scheme, which was conceived from a study of the population recovery of the ground state MbNO and its mutant (the A-state recovery), could simulate the IR data (kinetics of three states for the deligated NO) from MbNO in D_2O when the "minor" B_2 state was neglected and rebinding proceeds through B_0 rather than B_1.[28] On the contrary to their conclusion, when their three-state scheme was attempted, it severely deviated from the data regardless of whether the B_2 state was included in B_1 or neglected (see Figure 7a). Furthermore, although the B_2 state is

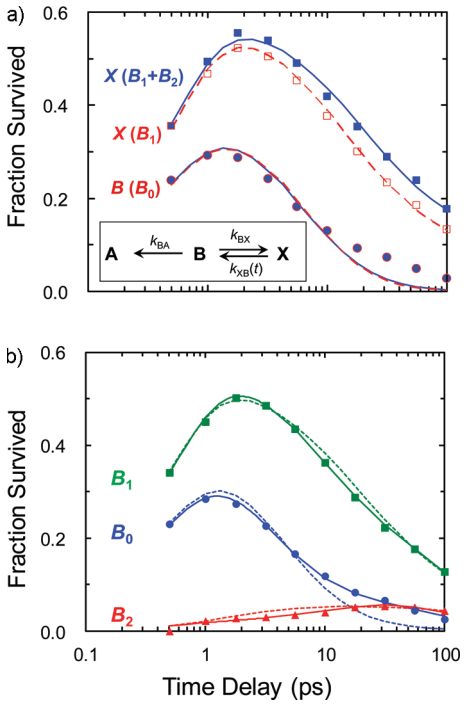

Figure 7. Time dependence of the integrated B-state absorbance of MbNO in D_2O. (a) The three-state scheme (A, B, X) proposed by Champion and co-workers,[28] where the B_0 state was labeled with B and the B_1 with X, whereas the B_2 state was neglected. Time-dependent changes in B and X were fitted using the proposed scheme (shown as an inset) when B_2 is added to X (blue symbols and blue solid line) and neglected (red symbols and red dotted line). (b) Best fit using the most general four-state (A, B_0, B_1, and B_2) kinetics model with the time-independent rebinding: a model with time-independent rebinding from all three states and time-dependent translocations between them (dotted lines). The fit using the four-state kinetic scheme incorporating time-dependent rebinding from B_1 and time-independent translocations between the three states is also shown for comparison (solid lines; from ref 14).

minor in the early time, it comprises more than 20% of the total remaining population at the later time and should not be neglected. A most general kinetics scheme with time-independent rebinding, a scheme containing time-independent rebinding from all three states and time-dependent translocations between them was evaluated to further check if the suggested time-independent rebinding can be used to describe the kinetics of the dissociated NO. As shown in Figure 7b, the most general time-independent rebinding scheme deviates strongly from the data, necessitating time-dependent rebinding. In the course of the fitting, it was found that the highly nonexponential decay character of each of the three B states cannot be reproduced by exponential rebinding even incorporating the nonexponential translocations between the three states. Clearly, the rebinding kinetics of NO from the B state is time-dependent, even though the A-state recovery kinetics appears to have a characteristic exponential time constant. The kinetics model proposed from this study has nonexponential rebinding and exponential translocations. The kinetics of the B state can be well described by the nonexponential translocations between the B states provided the rebinding is nonexponential. Regardless of whether the translocation is exponential or not, rebinding needs to be nonexponential to describe the observed kinetic behavior of the deligated NO. Interestingly, the present kinetics model can reproduce the A-state recovery kinetics of a distal-pocket mutated Mb (V68W), which has rebinding kinetics that lack the slow phase.[28] The kinetics of the mutant was used to support the three-state (A, B, and X) scheme by suggesting that the slower rate is related to the transitions from the Xe4 site to the heme pocket that is blocked by bulky W68 residing along the pathway from the heme pocket to the Xe4 site.[28] The optimized parameters for the kinetics of V68W from the present kinetics model have a negligible rebinding barrier, suggesting that V68 might be related to the barrier for NO rebinding. The optimized initial distribution of the NO showed two states for the deligated NO in the mutant in contrast with only one state for the dissociated NO in the three-state (A, B, and X) scheme. Proposed schemes would be readily evaluated by the time-resolved vibrational spectroscopy of the deligated NO from NO-bound V68W.

It was found that the more photon energy in the photolysis pulse increases the amplitude of the slow phase in the kinetics of GR of NO to Mb.[28] The four-states kinetics model suggested here can also explain the dependence of the GR kinetics on the photolysis photon energy if the higher photolysis energy produces more nascent population in the B_2 state. If the B_2 state is the farthest from the bound state, it requires more energy to reach the state. Although the present kinetics model is successful in explaining state-specific kinetics of the NO rebinding to Mb and Hb in various viscous solutions, it is not necessarily a unique scheme for NO rebinding to these proteins. However, it is a good working scheme that describes all the salient kinetic behaviors of the deligated NO as well as the population recovery of NO bound protein.

Effect of Conformational Changes on NO Rebinding. The viscosity-dependent GR of NO to Mb clearly demonstrates that the NO rebinding is coupled to the conformational relaxation and thus is nonexponential. The conformational changes are the main origins of the nonexponential behavior of the NO rebinding dynamics in Mb in room temperature solution. The kinetics model that is consistent with the time-dependent changes of all the B states and A state suggests that the conformational relaxation modifies the rebinding barrier from the B to A state. Although ligand migration might also be affected by a conformational change, the nonexponential GR of NO requires conformation-controlled rebinding barrier. The rate constants for conformational relaxation, which were probed by examining the change in the amide band of Mb that decreased from $(5.4\ \text{ps})^{-1}$ to $(10\ \text{ps})^{-1}$ with increasing solvent viscosity, showed the same trend but was larger than that for growth of the rebinding barrier of NO to Mb, ranging from $(14\ \text{ps})^{-1}$ to $(23\ \text{ps})^{-1}$. The rate constant for the conformational relaxation probed in the amide band of Hb was $(15\ \text{ps})^{-1}$, which is larger than that for the growth of the

dx.doi.org/10.1021/jp300176q | J. Phys. Chem. B 2012, 116, 5819−5830

rebinding barrier of NO to Hb, $(39\ ps)^{-1}$. Evidently, the amide band and growth of the rebinding barrier do not have the same structural origin but are related to each other.

The contribution of the conformation to the enthalpic barrier for the ligand rebinding to heme proteins has been categorized as a proximal effect[6,11] or a distal effect.[17,24,61−64] The proximal effect, originating mainly from the out-of-plane Fe motion and known to contribute to the rebinding of CO to Mb, was revoked in the GR of NO to Mb on the ps time scale at room temperature.[16,23,24] For example, on the basis of experiments on NO rebinding to the proximal-site modified mutant Mb and leghemoglobin, Kundu et al. suggested that the proximal effect on NO rebinding is negligible in both proteins up to 900 ps after photodissociation.[65] According to the harpoon mechanism introduced for NO rebinding to Mb, where the NO rebinds to the heme Fe in the out-of-plane conformation, the out-of-plane position of heme Fe make a negligible contribution to the enthalpic barrier of NO rebinding.[28] Since the proximal effect arises mainly from the energy needed to bring the heme Fe back to the heme plane by thermal fluctuations, if the NO rebinds to the Fe in the out-of-plane position, the proximal effect is negligible. The harpoon mechanism is consistent with a reactant-like transition state for NO rebinding[31] as well as the much faster NO rebinding rate than CO rebinding, where CO waits until thermal fluctuations drive the Fe into the heme plane prior to binding. A theoretical calculation also indicated that NO can bind to a domed Fe.[66] More recent fs resonance Raman and visible spectroscopy showed that the Fe motion to the heme plane did not follow the kinetics of NO rebinding and was delayed. This suggests that NO bound to a domed Fe and protein exerts structural constraints on heme causing the delayed Fe motion.[67] These experimental and theoretical observations suggest that the proximal effect in NO rebinding is negligible. According to several experiments on the NO rebinding dynamics of distal mutants, rebinding is affected strongly by a mutation in the distal site and the distal residues control NO motion, indicating that the distal effect makes a strong contribution to the time-dependent barrier on the GR of NO to Mb.[16,23,28,68−72] Time-resolved X-ray crystallography and molecular dynamics (MD) simulations showed that during CO migration residues near the active binding site propagate conformation changes, and ligand migration is coupled to the changes in protein conformation.[73−76] From the conformational changes, the residues near the distal active site can lead to steric hindrance for the rebinding of NO, suggesting that protein rearrangements can affect the NO rebinding dynamics and make it nonexponential. The successful kinetics model proposed in the present study has the rebinding process from the B_1 state, which has a time-dependent barrier. The rebinding barrier of NO likely arises from the steric hindrance caused by residues in the distal side of the heme pocket during NO rebinding from the B_1 state to A state. The barrier becomes time-dependent as the residues rearrange with conformational relaxation after deligation.

Assignment of B States. Multiple vibrational bands for the bound ligand (A states) result from different ligand-bound protein conformations (conformational substates), and those for the deligated ligand (B states) originate from different positions and/or orientations of the ligand within a protein in a given conformational substate.[13,14,50,77] Two vibrational bands for MbNO suggest that MbNO has at least two conformational substates.[13,14,50,77] The three vibrational bands for the dissociated NO in MbNO (three B states) suggest that the deligated NO resides in at least three different locations within Mb, two different locations one of which has two different orientations, or one location with three different orientations. Time-resolved vibrational spectroscopy alone cannot determine the precise sites for the deligated NO, but a few possible sites for the location of the deligated NO can be proposed by comparatively analyzing the data with previous reports on an analysis of the MbCO data, MD simulations, and an analysis of the MbNO data at cryogenic temperatures.[48,78−80] As shown in Figure 8, the B-state spectra were also observed for either horse

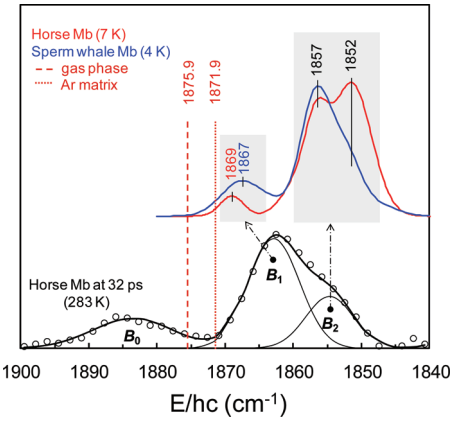

Figure 8. Spectra for the photodeligated NO from MbNO. Time-resolved spectrum at a delay time of 32 ps after the photolysis of horse MbNO at 283 K (black symbols and lines) is shown with its decomposed components. The offset bands are the FT-IR spectra obtained by photolyzing either horse MbNO at 7 K for 5 min with a white light source (red solid line)[78] or sperm whale Mb at 4 K for 20 s using a 532 nm laser (blue solid lines).[48] The peak position of each band in the FT-IR spectra was marked. The dash-dotted arrows are shown to relate the bands at room temperature with those in the shaded area at low temperatures. The positions of the vibrational band of NO in the gas phase (brown dashed line)[81] and solid Ar matrix (brown dotted line) were also shown for comparison.[82,83]

Mb at 7 K photolyzed for 5 min using a white light source[78] or sperm whale Mb (swMb) at 4 K photolyzed for 20 s with a 532 nm laser.[48] Both spectra showed three bands; a minor band at 1867 or 1869 cm^{-1} and two major bands peaked at 1857 and 1852 cm^{-1}. Although the positions of the three bands were similar, their relative magnitudes and widths appeared to be different. The difference in magnitude can arise from the different degree of rebinding from and/or different initial partitioning of the deligated ligand into the corresponding site, which might result from either species variations or a different photolysis protocol. All the bands in these spectra were red-shifted not only from the vibrational band of NO in the gas phase, 1875.9 cm^{-1}, but also from that in the solid Ar matrix, 1871.9 cm^{-1},[81−83] which are similar environments to the nonpolar protein interior. While ignoring the minor band at 1869 cm^{-1}, the two major bands at 1857 and 1852 cm^{-1} observed in horse Mb at 7 K were attributed to NO in the opposite orientation in the primary docking site.[78] The bands at 1867 and 1857 cm^{-1} observed in sw-Mb at 4 K were assigned to NO in two different orientations in the primary docking site based on a comparative study of the NO- and CO-ligated Mb and Mb mutants by FT-IR spectroscopy and temperature derivative spectroscopy.[48] The large splitting (10 cm^{-1}) was suggested to arise from an electrostatic interaction between NO and His-64. The small splitting in the two major bands (1857

dx.doi.org/10.1021/jp300176q | J. Phys. Chem. B 2012, 116, 5819−5830

and 1852 cm^{-1}) in swMb was explained either by two bound-state conformations or additional NO orientations in the primary docking site.[48] The red-shifted vibrational bands observed at cryogenic temperatures were quite similar to the red-shifted B_1 and B_2 bands in the present data. Therefore, the B_1 and B_2 bands can be attributed to NO in the opposite orientation in the primary docking site. The splitting of 7.3−9 cm^{-1} between the B_1 and B_2 bands is comparable to the 10−12 cm^{-1} observed at cryogenic temperatures. The small splitting in the two major bands observed at low temperatures was not resolved in the room-temperature data, possibly due to the broadening of the band.

The photon energy used for photodeligation was much higher than that required to break the Fe−NO bond. Therefore, the excess energy heats up the heme by a few hundreds of degrees, even for the sample at cryogenic temperatures.[84] The heated heme cools on a ps time scale,[84−86] and the deligated NO is sandwiched between a hot heme and cold protein during thermal relaxation. In the experiment at cryogenic temperatures, NO likely rebinds from the B_1 state during thermal relaxation and is eventually quenched in a low-temperature population distribution that is not in thermal equilibrium but kinetically trapped. Efficient ps rebinding from the B_1 state can explain the much smaller band near 1868 cm^{-1} in the low-temperature data.

The B_0 band, which was blue-shifted from that in the gas phase, was not observed in the low-temperature data, suggesting that the NO in the B_0 state is unstable, rebinds rapidly, and/or translocates into the B_1 state.[14] The vibrational band of NO was blue-shifted when its N atom was hydrogen bonded.[87,88] The hydrogen bond between the N atom of NO and the distal histidine was suggested to explain the blue-shifted B_0 band.[14] According to recent MD simulations of the photodeligated NO, deligated NO remains mainly in the center of the distal heme pocket where NO can readily form a hydrogen bond with the distal histidine.[79] The primary docking site was located further from the distal histidine than the distal heme pocket.[79] Therefore, the distal histidine may not form a normal hydrogen bond with the ligand in the primary docking site.[89,90] Interestingly, the calculated IR bands for the photodeligated NO in the simulation were blue-shifted by 1−8 cm^{-1} compared to the gas-phase value, which corroborates the assignment of the B_0 band to NO in the distal heme pocket.[79]

The deligated NO was suggested to migrate to the Xe4 site, which is a secondary photoproduct site observed in a protein with high-pressure Xe.[30,91] When MbNO was photolyzed continuously, while slowly cooling the sample from 160 to 4 K, most of the NO was photolyzed and the vibrational spectrum showed two vibrational bands at 1869 and 1865 cm^{-1}.[48] The majority of NO observed in this low-temperature experiment is believed to have been trapped in the secondary site. As mentioned above, since NO in the primary docking site can rebind on a ps time scale, the slow cooing protocol results mainly in trapped NO in the Xe4 site. On the other hand, most of this NO will rebind before reaching the Xe4 site of Mb under physiological conditions if the motion of NO into the Xe4 site takes longer than 100 ps at room temperature. This is because a majority of the deligated NO rebinds to Mb at room temperature within 100 ps. Recent MD simulations on the rebinding dynamics of NO to Mb using a new surface-crossing algorithm reported that the NO observed in the Xe4 site were the ones that do not rebind within 1 ns.[80] It was suggested that NO molecules that rebind after 500 ps visit the Xe4 site.[80] Many experimental and theoretical studies on the migration of CO after photolysis from MbCO indicated that the deligated CO resides in the primary docking site for longer than tens of nanoseconds before moving to the Xe4 site.[73−75,92−94] Evidently, it appears to take more than hundreds of picoseconds for either CO or NO to move to the Xe4 site from the primary docking site in Mb at room temperature. Therefore, most of deligated NO under physiological conditions likely rebinds from the primary docking site before visiting the Xe4 site. Therefore, the spectrum observed at room temperature arises mainly from NO in the center of distal pocket[79] and/or the primary docking site. Although the kinetics of NO indicates that the B states are not from NO in the Xe4 site, the possibility that some of the vibrational bands observed in MbNO at room temperature can be assigned to NO in the secondary sites, such as the Xe4 or the Xe1 site, cannot be excluded because the band position for the NO in the Xe4 pocket is similar to that in the B states.[48] This issue can be clarified by ps time-resolved X-ray crystallography at room temperature.

V. CONCLUSION

Femtosecond vibrational spectroscopy was used to probe simultaneously the GR kinetics of NO to Mb and Hb as well as their conformational relaxation after deligation as a function of the solvent viscosity. The kinetics of GR of NO to the heme proteins was inverse correlated with that of the conformational relaxation of the corresponding protein. The inverse correlation suggests that the rebinding of NO is retarded by conformational relaxation, suggesting that the rebinding barrier increases with the conformational relaxation of the protein. The rebinding kinetics of the deligated NO within the Mb dissolved in a viscous solution, which were observed after the photodeligation of MbNO in the 48 wt % G/W mixture, was virtually identical to that observed in MbNO in D_2O except for the faster decay kinetics. The state-specific kinetics of the deligated NO (B_0, B_1, and B_2 state) and the recovery kinetics of the bleach spectra of MbNO (A state) were most consistent with a kinetics model involving four states (A, B_0, B_1, and B_2), which incorporates a time-dependent rebinding barrier from B_1 with exponential translocations between three B states. Using this kinetic model, the rate constants for the translocations between the three B states were found to be independent of the solvent viscosity, and only the rate constant for the growth of the rebinding barrier (k_{bar}) decreased in the viscous solution. All the GR dynamics of NO to Mb and Hb in various viscous solutions were well described by the proposed four-state kinetics model with k_{bar} decreasing with increasing solvent viscosity, whereas all other fitting parameters were the same for the corresponding protein in D_2O. The spectral characteristics of the deligated NO were compared with those at cryogenic temperatures together with the reported MD simulations on MbNO. From this analysis, B_0 was assigned to the NO in the center of distal pocket observed in a MD simulations[79] and the remaining two B states (B_1 and B_2) were assigned to the NO in the primary docking site in the opposite orientation. We envisioned that the photodeligated NO rebinds from the primary docking site, and rebinding barrier, which is likely the result of steric hindrance due to residues in the distal side of the heme, increased with the conformational relaxation that can be retarded by a viscous solvent. The GR of NO to Mb is accelerated in a viscous solution because the ps conformational

dx.doi.org/10.1021/jp300176q | J. Phys. Chem. B 2012, 116, 5819−5830

relaxation of Mb is retarded by a viscous solvent and its rate is comparable to the rebinding rate of NO. On the other hand, the ps conformational relaxation of Hb is delayed by the quaternary structure of Hb. Moreover, its rate is slower than the rebinding rate of NO, which results in negligible viscosity-dependency of the GR of NO to Hb.

AUTHOR INFORMATION

Corresponding Author

*E-mail: mhlim@pusan.ac.kr.

Notes

The authors declare no competing financial interest.

ACKNOWLEDGMENTS

This work was supported by the Basic Science Research Program through the National Research Foundation of Korea funded by the Ministry of Education, Science and Technology (2011-0016114).

REFERENCES

(1) Austin, R. H.; Beeson, K. W.; Eisenstein, L.; Frauenfelder, H.; Gunsalus, I. C. *Biochemistry* **1975**, *14*, 5355.
(2) Chernoff, D. A.; Hochstrasser, R. M.; Steele, A. W. *Proc. Natl. Acad. Sci. U. S. A.* **1980**, *77*, 5606.
(3) Henry, E. R.; Sommer, J. H.; Hofrichter, J.; Eaton, W. A. *J. Mol. Biol.* **1983**, *166*, 443.
(4) Pin, S.; Valat, P.; Tourbez, H.; Alpert, B. *Chem. Phys. Lett.* **1986**, *128*, 79.
(5) Ansari, A.; Berendzen, J.; Braunstein, D. K.; Cowen, B. R.; Frauenfelder, H.; Hong, M. K.; Iben, I. E. T.; Johnson, J. B.; Ormos, P.; et al. *Biophys. Chem.* **1987**, *26*, 337.
(6) Petrich, J. W.; Poyart, C.; Martin, J. L. *Biochemistry* **1988**, *27*, 4049.
(7) Findsen, E. W.; Ondrias, M. R. *Photochem. Photobiol.* **1990**, *51*, 741.
(8) Springer, B. A.; Sligar, S. G.; Olson, J. S.; Phillips, G. N., Jr. *Chem. Rev.* **1994**, *94*, 699.
(9) Henry, E. R.; Jones, C. M.; Hofrichter, J.; Eaton, W. A. *Biochemistry* **1997**, *36*, 6511.
(10) Case, D. A.; Karplus, M. *J. Mol. Biol.* **1979**, *132*, 343.
(11) Petrich, J. W.; Lambry, J. C.; Kuczera, K.; Karplus, M.; Poyart, C.; Martin, J. L. *Biochemistry* **1991**, *30*, 3975.
(12) Shreve, A. P.; Franzen, S.; Simpson, M. C.; Dyer, R. B. *J. Phys. Chem. B* **1999**, *103*, 7969.
(13) Kim, S.; Jin, G.; Lim, M. *J. Phys. Chem. B* **2004**, *108*, 20366.
(14) Kim, S.; Lim, M. *J. Am. Chem. Soc.* **2005**, *127*, 8908.
(15) Jongeward, K. A.; Magde, D.; Taube, D. J.; Marsters, J. C.; Traylor, T. G.; Sharma, V. S. *J. Am. Chem. Soc.* **1988**, *110*, 380.
(16) Gibson, Q. H.; Regan, R.; Elber, R.; Olson, J. S.; Carver, T. E. *J. Biol. Chem.* **1992**, *267*, 22022.
(17) Petrich, J. W.; Lambry, J. C.; Balasubramanian, S.; Lambright, D. G.; Boxer, S. G.; Martin, J. L. *J. Mol. Biol.* **1994**, *238*, 437.
(18) Walda, K. N.; Liu, X. Y.; Sharma, V. S.; Magde, D. *Biochemistry* **1994**, *33*, 2198.
(19) Schaad, O.; Zhou, H. X.; Szabo, A.; Eaton, W. A.; Henry, E. R. *Nat. Struct. Biol.* **1993**, *90*, 9547.
(20) Agmon, N.; Hopfield, J. J. *J. Chem. Phys.* **1983**, *79*, 2042.
(21) Srajer, V.; Reinisch, L.; Champion, P. M. *J. Am. Chem. Soc.* **1988**, *110*, 6656.
(22) Steinbach, P. J.; Ansari, A.; Berendzen, J.; Braunstein, D.; Chu, K.; Cowen, B. R.; Ehrenstein, D.; Frauenfelder, H.; Johnson, J. B.; et al. *Biochemistry* **1991**, *30*, 3988.
(23) Ikeda-Saito, M.; Dou, Y.; Yonetani, T.; Olson, J. S.; Li, T.; Regan, R.; Gibson, Q. H. *J. Biol. Chem.* **1993**, *268*, 6855.
(24) Kholodenko, Y.; Gooding, E. A.; Dou, Y.; Ikeda-Saito, M.; Hochstrasser, R. M. *Biochemistry* **1999**, *38*, 5918.
(25) Meuwly, M.; Becker, O. M.; Stote, R.; Karplus, M. *Biophys. Chem.* **2002**, *98*, 183.
(26) Tian, W. D.; Sage, J. T.; Srajer, V.; Champion, P. M. *Phys. Rev. Lett.* **1992**, *68*, 408.
(27) Lambright, D. G.; Balasubramanian, S.; Boxer, S. G. *Biochemistry* **1993**, *32*, 10116.
(28) Ionascu, D.; Gruia, F.; Ye, X.; Yu, A.; Rosca, F.; Beck, C.; Demidov, A.; Olson, J. S.; Champion, P. M. *J. Am. Chem. Soc.* **2005**, *127*, 16921.
(29) Lim, M.; Jackson, T. A.; Anfinrud, P. A. *J. Chem. Phys.* **1995**, *102*, 4355.
(30) Tilton, R. F., Jr.; Kuntz, I. D., Jr.; Petsko, G. A. *Biochemistry* **1984**, *23*, 2849.
(31) Szabo, A. *Proc. Natl. Acad. Sci. U. S. A.* **1978**, *75*, 2108.
(32) Jackson, T. A.; Lim, M.; Anfinrud, P. A. *Chem. Phys.* **1994**, *180*, 131.
(33) Causgrove, T. P.; Dyer, R. B. *Biochemistry* **1993**, *32*, 11985.
(34) Causgrove, T. P.; Dyer, R. B. *J. Phys. Chem.* **1996**, *100*, 3273.
(35) Kim, S.; Jin, G.; Lim, M. *Bull. Korean Chem. Soc.* **2003**, *24*, 1470.
(36) Perutz, M. F.; Mathews, F. S. *J. Mol. Biol.* **1966**, *21*, 199.
(37) Takano, T. *J. Mol. Biol.* **1977**, *110*, 569.
(38) Lim, M.; Wolford, M. F.; Hamm, P.; Hochstrasser, R. M. *Chem. Phys. Lett.* **1998**, *290*, 355.
(39) Hamm, P.; Lim, M.; Hochstrasser, R. M. *J. Phys. Chem. B* **1998**, *102*, 6123.
(40) Hamm, P.; Kaindl, R. A.; Stenger, J. *Opt. Lett.* **2000**, *25*, 1798.
(41) Lim, M. *Bull. Korean Chem. Soc.* **2002**, *23*, 865.
(42) Moller, J. K. S.; Skibsted, L. H. *Chem. Rev.* **2002**, *102*, 1167.
(43) Hamm, P. *Chem. Phys.* **1995**, *200*, 415.
(44) Wynne, K.; Hochstrasser, R. M. *Chem. Phys.* **1995**, *193*, 211.
(45) Dong, A.; Huang, P.; Caughey, W. S. *Biochemistry* **1990**, *29*, 3303.
(46) Dousseau, F.; Pezolet, M. *Biochemistry* **1990**, *29*, 8771.
(47) Kim, S.; Park, J.; Lee, T.; Lim, M. Manuscript in preparation.
(48) Nienhaus, K.; Palladino, P.; Nienhaus, G. U. *Biochemistry* **2008**, *47*, 935.
(49) Bevington, P. R. *Data Reduction and Error Analysis for the Physical Sciences*; McGraw-Hill Book Co.: New York, 1969.
(50) Mourant, J. R.; Braunstein, D. P.; Chu, K.; Frauenfelder, H.; Nienhaus, G. U.; Ormos, P.; Young, R. D. *Biophys. J.* **1993**, *65*, 1496.
(51) Lim, M.; Jackson, T. A.; Anfinrud, P. A. *Nat. Struct. Biol.* **1997**, *4*, 209.
(52) Olson, J. S.; Phillips, G. N., Jr. *J. Biol. Chem.* **1996**, *271*, 17593.
(53) Ye, X.; Demidov, A.; Champion, P. M. *J. Am. Chem. Soc.* **2002**, *124*, 5914.
(54) Kim, S.; Lim, M. *Bull. Korean Chem. Soc.* **2006**, *27*, 1825.
(55) Brooks, C. L., III; Karplus, M.; Petitt, B. M. *Proteins: A Theoretical Perspective of Dynamics, Structure and Thermodynamics*; John Wiley & Sons: New York, 1988.
(56) Wang, Y.; Baskin, J. S.; Xia, T.; Zewail, A. H. *Proc. Natl. Acad. Sci. U. S. A.* **2004**, *101*, 18000.
(57) Kuczera, K.; Lambry, J. C.; Martin, J. L.; Karplus, M. *Proc. Natl. Acad. Sci. U. S. A.* **1993**, *90*, 5805.
(58) Lim, M.; Jackson, T. A.; Anfinrud, P. A. *Proc. Natl. Acad. Sci. U. S. A.* **1993**, *90*, 5801.
(59) Adachi, S.-i.; Park, S.-Y.; Tame, J. R. H.; Shiro, Y.; Shibayama, N. *Proc. Natl. Acad. Sci. U. S. A.* **2003**, *100*, 7039.
(60) Eaton, W. A.; Henry, E. R.; Hofrichter, J.; Mozzarelli, A. *Nat. Struct. Biol.* **1999**, *6*, 351.
(61) Negrerie, M.; Bouzhir, L.; Martin, J.-L.; Liebl, U. *J. Biol. Chem.* **2001**, *276*, 46815.
(62) Franzen, S.; Lambry, J. C.; Bohn, B.; Poyart, C.; Martin, J. L. *Nat. Struct. Biol.* **1994**, *1*, 230.
(63) Franzen, S.; Bohn, B.; Poyart, C.; DePillis, G.; Boxer, S. G.; Martin, J.-L. *J. Biol. Chem.* **1995**, *270*, 1718.
(64) Duprat, A. F.; Traylor, T. G.; Wu, G. Z.; Coletta, M.; Sharma, V. S.; Walda, K. N.; Magde, D. *Biochemistry* **1995**, *34*, 2634.
(65) Kundu, S.; Snyder, B.; Das, K.; Chowdhury, P.; Park, J.; Petrich, J. W.; Hargrove, M. S. *Proteins: Struct., Funct., Genet.* **2002**, *46*, 268.

(66) Franzen, S. *Proc. Natl. Acad. Sci. U. S. A.* **2002**, *99*, 16754.
(67) Kruglik, S. G.; Yoo, B.-K.; Franzen, S.; Vos, M. H.; Martin, J.-L.; Negrerie, M. *Proc. Natl. Acad. Sci. U. S. A.* **2010**, *107*, 13678.
(68) Carver, T. E.; Rohlfs, R. J.; Olson, J. S.; Gibson, Q. H.; Blackmore, R. S.; Springer, B. A.; Sligar, S. G. *J. Biol. Chem.* **1990**, *265*, 20007.
(69) Carlson, M. L.; Regan, R.; Elber, R.; Li, H.; Phillips, G. N., Jr.; Olson, J. S.; Gibson, Q. H. *Biochemistry* **1994**, *33*, 10597.
(70) Quillin, M. L.; Li, T.; Olson, J. S.; Phillips, G. N., Jr.; Dou, Y.; Ikeda-Saito, M.; Regan, R.; Carlson, M.; Gibson, Q. H.; et al. *J. Mol. Biol.* **1995**, *245*, 416.
(71) Nienhaus, K.; Deng, P.; Kriegl, J. M.; Nienhaus, G. U. *Biochemistry* **2003**, *42*, 9647.
(72) Nienhaus, K.; Deng, P.; Olson, J. S.; Warren, J. J.; Nienhaus, G. U. *J. Biol. Chem.* **2003**, *278*, 42532.
(73) Schotte, F.; Lim, M.; Jackson, T. A.; Smirnov, A. V.; Soman, J.; Olson, J. S.; Phillips, G. N., Jr.; Wulff, M.; Anfinrud, P. A. *Science* **2003**, *300*, 1944.
(74) Hummer, G.; Schotte, F.; Anfinrud, P. A. *Proc. Natl. Acad. Sci. U. S. A.* **2004**, *101*, 15330.
(75) Schotte, F.; Soman, J.; Olson, J. S.; Wulff, M.; Anfinrud, P. A. *J. Struct. Biol.* **2004**, *147*, 235.
(76) Schmidt, M.; Nienhaus, K.; Pahl, R.; Krasselt, A.; Anderson, S.; Parak, F.; Nienhaus, G. U.; Srajer, V. *Proc. Natl. Acad. Sci. U. S. A.* **2005**, *102*, 11704.
(77) Nienhaus, K.; Nienhaus, G. U. *Biochim. Biophys. Acta, Proteins Proteomics* **2011**, *1814*, 1030.
(78) Miller, L. M.; Pedraza, A. J.; Chance, M. R. *Biochemistry* **1997**, *36*, 12199.
(79) Nutt, D. R.; Meuwly, M. *ChemPhysChem* **2004**, *5*, 1710.
(80) Nutt, D. R.; Meuwly, M. *Biophys. J.* **2006**, *90*, 1191.
(81) Herzberg, G. *Molecular Spectra and Molecular Structure: Spectra of Diatomic Molecules*; Van Nostrand Reinhold: New York, 1950.
(82) Bhatia, S. C.; Hall, J. H. *J. Phys. Chem.* **1980**, *84*, 3255.
(83) Frei, H.; Pimentel, G. C. *J. Phys. Chem.* **1981**, *85*, 3355.
(84) Henry, E. R.; Eaton, W. A.; Hochstrasser, R. M. *Proc. Natl. Acad. Sci. U. S. A.* **1986**, *83*, 8982.
(85) Lingle, R., Jr.; Xu, X.; Zhu, H.; Yu, S. C.; Hopkins, J. B. *J. Phys. Chem.* **1991**, *95*, 9320.
(86) Lim, M.; Jackson, T. A.; Anfinrud, P. A. *J. Phys. Chem.* **1996**, *100*, 12043.
(87) Krim, L.; Alikhani, M. E. *Chem. Phys.* **1998**, *237*, 265.
(88) Rensberger, K. J.; Blair, J. T.; Weinhold, F.; Crim, F. F. *J. Chem. Phys.* **1989**, *91*, 1688.
(89) Chu, K.; Vojtchovsky, J.; McMahon, B. H.; Sweet, R. M.; Berendzen, J.; Schlichting, I. *Nature* **2000**, *403*, 921.
(90) Lim, M.; Jackson, T. A.; Anfinrud, P. A. *J. Am. Chem. Soc.* **2004**, *126*, 7946.
(91) Tilton, R. F., Jr.; Singh, U. C.; Weiner, S. J.; Connolly, M. L.; Kuntz, I. D., Jr.; Kollman, P. A.; Max, N.; Case, D. A. *J. Mol. Biol.* **1986**, *192*, 443.
(92) Henry, E. R.; Levitt, M.; Eaton, W. A. *Proc. Natl. Acad. Sci. U. S. A.* **1985**, *82*, 2034.
(93) Srajer, V.; Ren, Z.; Teng, T.-Y.; Schmidt, M.; Ursby, T.; Bourgeois, D.; Pradervand, C.; Schildkamp, W.; Wulff, M.; Moffat, K. *Biochemistry* **2001**, *40*, 13802.
(94) Bourgeois, D.; Vallone, B.; Schotte, F.; Arcovito, A.; Miele, A. E.; Sciara, G.; Wulff, M.; Anfinrud, P.; Brunori, M. *Proc. Natl. Acad. Sci. U. S. A.* **2003**, *100*, 8704.